The electrochemical oxidation and reduction of nitrate ions in the room temperature ionic liquid [C_2mim][NTf_2]; the latter behaves as a 'melt' rather than an 'organic solvent'

Tessa L. Broder,[a] Debbie S. Silvester,[a] Leigh Aldous,[b] Christopher Hardacre,[b] Alison Crossley[c] and Richard G. Compton*[a]

Received (in Montpellier, France) 24th January 2007, Accepted 23rd March 2007
First published as an Advance Article on the web 17th April 2007
DOI: 10.1039/b701097d

The electrochemical oxidation of 1-butyl-3-methylimidazolium nitrate [C_4mim][NO_3] was studied by cyclic voltammetry in the room temperature ionic liquid (RTIL) 1-ethyl-3-methylimidazolium bis(trifluoromethylsulfonyl)imide [C_2mim][NTf_2]. A sharp peak was observed on a Pt microelectrode (d = 10 μm), and a diffusion coefficient at infinite dilution of *ca.* 2.0×10^{-11} m^2 s^{-1} was obtained. Next, the cyclic voltammetry of sodium nitrate ($NaNO_3$) and potassium nitrate (KNO_3) was studied, by dissolving small amounts of solid into the RTIL [C_2mim][NTf_2]. Similar oxidation peaks were observed, revealing diffusion coefficients of *ca.* 8.8 and 9.0×10^{-12} m^2 s^{-1} and solubilities of 11.9 and 10.8 mM for $NaNO_3$ and KNO_3, respectively. The smaller diffusion coefficients for $NaNO_3$ and KNO_3 (compared to [C_4mim][NO_3]) may indicate that NO_3^- is ion-paired with Na^+ or K^+. This work may have applications in the electroanalytical determination of nitrate in RTIL solutions. Furthermore, a reduction feature was observed for both $NaNO_3$ and KNO_3, with additional anodic peaks indicating the formation of oxides, peroxides, superoxides and nitrites. This behaviour is surprisingly similar to that obtained from melts of $NaNO_3$ and KNO_3 at high temperatures (*ca.* 350–500 °C), and this observation could significantly simplify experimental conditions required to investigate these compounds. We then used X-ray photoelectron spectroscopy (XPS) to suggest that disodium(I) oxide (Na_2O), which has found use as a storage compound for hydrogen, was deposited on a Pt electrode surface following the reduction of $NaNO_3$.

Introduction

Over the past century, many researchers have realised the importance of studying the reduction of nitrate (NO_3^-) ions, due to their potentially damaging effect on the environment. Most nitrates are highly water soluble, and may lead to severe environmental and health hazards if present in ground water at high concentrations. This has led to many studies focusing on the analytical determination of nitrate (and nitrite, NO_2^-) ion concentrations.[1] Various salts of nitrates are also used commercially for many applications, such as in the production of ammonia gas,[2–4] and of hydroxylamine,[2,4] a valuable raw material in the chemical industry.

Many researchers have reported the catalysed electrochemical reduction of nitrate ions in acidic media,[2,5] but the mechanisms proposed are complicated by the presence of protons from the solvent. Several other reports[6–9] have focused on the cyclic voltammetry obtained from melts of several nitrate salts. The main advantage of studying a melt is that the solution is not contaminated by any proton donor species, or by any supporting electrolyte, since the solutions are intrinsically conductive (made entirely of ions). However, the need for high temperatures (*ca.* 250–500 °C) is a major drawback in the ease and safety of the experimental set-up.

The suggested mechanism[7,8,10,11] for the reduction of nitrate is given by eqn (1), resulting in the formation of oxide ions (O^{2-}).

$$MNO_3 + 2e^- \rightarrow MNO_2 + O^{2-} \quad (1)$$

In acidic solutions,[2,5] the reaction occurs in the presence of protons, which catalyse the reaction and lead to the formation of water, as opposed to the oxide ion. However, when the ions are in a proton deficient environment, such as in a melt, several authors[7–9] have suggested the formation of oxide, peroxide and superoxide species of the corresponding cations (*e.g.* lithium, sodium and potassium), following the reduction. Several of these compounds are important in the chemical industry, in particular, sodium oxide (Na_2O), which has been shown to possess properties suitable for hydrogen storage.[12]

RTILs are liquids composed entirely of ions, and exist in the liquid state at and around room temperature. They possess typical properties such as high thermal stability, high viscosity, low-volatility, intrinsic conductivity, and wide electrochemical

[a] *Physical and Theoretical Chemistry Laboratory, University of Oxford, South Parks Road, Oxford, UK OX1 3QZ. E-mail: richard.compton@chemistry.oxford.ac.uk; Fax: +44 (0) 1865 275 410; Tel: +44 (0) 1865 275 413*
[b] *School of Chemistry and Chemical Engineering/QUILL, Queen's University Belfast, Belfast, Northern Ireland, UK BT9 5AG*
[c] *Department of Materials, University of Oxford Begbroke Business and Science Park, Sandy Lane, Yarnton, Oxford, UK OX5 1PF*

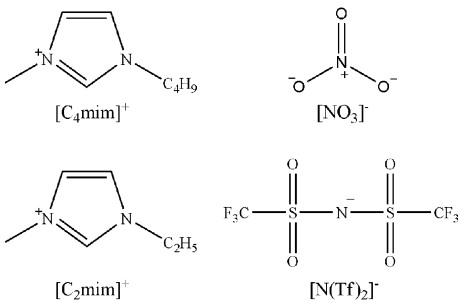

Fig. 1 Molecular structures of the RTIL cations and anions employed in this study.

windows. Much work has been reported using RTILs as solvents to replace conventional aprotic solvents (*e.g.* acetonitrile) in electrochemical experiments,[13] and also in many electrochemical applications, such as lithium batteries,[14] electrochemical sensors,[15] capacitors[16] and solar cells.[17]

In the present report, we show how the electrochemistry of $NaNO_3$ and KNO_3, dissolved in a room temperature ionic liquid (RTIL) at ambient temperatures (*ca.* 25 °C), compares surprisingly well with that obtained from melts of the same compounds at much higher temperatures (350–500 °C).[8] We report the electrochemistry of both sodium nitrate ($NaNO_3$) and potassium nitrate (KNO_3) in the room temperature ionic liquid 1-ethyl-3-methylimidazolium bis(trifluoromethylsulfonyl)imide [C_2mim][NTf_2] (see Fig. 1), which may prove to be significant in both the analytical determination of nitrate, and in the application of RTILs as electrolytes in batteries.

Experimental

Chemicals

1-Ethyl-3-methylimidazolium bis(trifluoromethylsulfonyl) imide ([C_2mim][NTf_2]) was prepared in house following a standard procedure reported in the literature.[18] The synthesis of 1-butyl-3-methylimidazolium nitrate ([C_4mim][NO_3]) was adapted from a previously published procedure.[19] $AgNO_3$ (5.36 g, 0.032 mol) and [C_4mim]Cl (5.00 g, 0.029 mol) were dissolved separately in minimum amounts of ultrapure water. The [C_4mim]Cl solution was then slowly added to the stirred $AgNO_3$ solution. After stirring overnight, the solution was filtered to remove the AgCl precipitate, the water removed and the IL dried under high vacuum at 70 °C overnight. The IL was then dissolved in 400 ml dry methanol, small amounts of activated charcoal and acidic alumina were added as seeds for the remaining AgCl, and the solution left overnight in a freezer. This solution was then filtered and the process repeated. The methanol was removed, and the ionic liquid was dried under high vacuum conditions. Ferrocene (Aldrich, 98%), tetrabutylammonium perchlorate (TBAP, Fluka, Puriss electrochemical grade, >99%), acetonitrile (Fischer Scientific, dried and distilled, >99.99%), sodium nitrate ($NaNO_3$, Fisons), potassium nitrate (KNO_3, Aldrich, >99%), sodium nitrite ($NaNO_2$, Aldrich, ≥ 97%), potassium nitrite (KNO_2, Aldrich, ≥ 96%), sodium oxide (Na_2O, Aldrich, 80%) and sodium peroxide (Na_2O_2, Aldrich, reagent grade, 97%) were used as received, without further purification.

Instrumental

Preparation of stock solutions. Saturated solutions of $NaNO_3$ and KNO_3 were prepared by dissolving approximately 2 mg of solid in 1.5 ml of [C_2mim][NTf_2]. The solutions were stirred for approximately 24 h to allow for full dissolution. Saturated solutions of $NaNO_2$ and KNO_2 were also prepared in the same way.

Electrochemical experiments. Cyclic voltammetry was performed using a computer controlled μ-Autolab potentiostat (Eco-Chemie, Netherlands). A conventional two-electrode arrangement was employed, with a platinum electrode (10 μm diameter) as the working electrode and a 0.5 mm diameter silver wire quasi-reference electrode. The electrodes were housed in a glass "T-cell"[20] specifically designed for examining microsamples of RTILs under a controlled atmosphere. The microelectrode was modified with a section of disposable micropipette tip, creating a small cavity above the disk into which 20–82 μL of ionic liquid was placed. For $NaNO_3$ and KNO_3, 20 μL of the saturated stock solutions (described above) were used. For [C_4mim][NO_3], the four solutions with concentrations of 1153, 524, 275 and 141 mM were prepared by adding 5, 2, 2 and 2 μL of [C_4mim][NO_3] to 20, 20, 40 and 80 μL of [C_2mim][NTf_2], respectively). For experiments using the larger platinum-disk working electrode (see below), a three-electrode arrangement was employed, with a 0.3 mm silver wire as a quasi-reference electrode, and a thin platinum coil as a counter electrode. The electrodes were housed in a cell designed for holding 1–3 ml of (previously degassed) solution, and were placed in the solution through a Teflon cap with four holes. A nitrogen line was fed through the fourth hole, and the top of the cell was covered to create an inert atmosphere above the solution.

The microelectrode was polished on soft lapping pads (Kemet Ltd, UK) using 1.0 μm and 0.3 μm aqueous-alumina slurries (Buehler, Illinois). The microdisk radius was calibrated electrochemically by analysing the steady-state voltammetry of a 2 mM solution of ferrocene in acetonitrile, containing 0.1 M TBAP as a supporting electrolyte, using a value for the diffusion coefficient of 2.3×10^{-9} m^2 s^{-1} at 298 K.[21]

Electrode design and XPS. A 6 mm diameter (1 mm thick) Pt disk was contained in an 8 mm cylindrical block of PTFE (4.5 mm thick) and mounted on a metal stub. The stub was made with the correct dimensions to be held easily inside the UHV chamber. Electrical contact to the Pt disk was made through the centre of the stub *via* a copper wire with a plastic coating. The surface of the electrode was cleaned with a small amount of acetone on tissue paper. After electrochemical experiments were performed, the wire was cut at the base of the stub. The electrode was removed from the ionic liquid, sprayed rapidly with acetone to remove liquid residues and introduced into the instrument *via* a turbo molecular pumped entry lock. The entry lock was pumped for about 30 min before the electrode was introduced into the analysis chamber. XPS was performed in an ion pumped UHV chamber equipped with a VG nine channel CLAM4 electron energy analyser (base pressure 5×10^{-10} torr). 250 watt unmonochromated Mg X-ray excitation

was used. The CLAM 4 has variable slits for small area analysis. The largest slit (5 mm) was used in this case, with no apertures selected. The analyser was operated at constant pass energy of 100 eV for wide scans. Detailed scans with the analyser operating at 20 eV pass energy were taken over the Pt 4f and the Na 1s peaks. Data were obtained using a VGX900-W operating system. Peak positions were obtained by setting the main C 1s peak to be 284.8 eV to compensate for charge shifting. Peak areas were measured after background subtraction following the methods of Shirley,[22] divided by an empirically derived sensitivity factor,[23] and normalised to give atomic percentages. We note here that a strong stream of acetone was necessary to remove most of the ionic liquid sample from the surface of the electrode, since otherwise the C, N, O, F and S peaks swamped the smaller Na and Pt peaks.

Chronoamperometric experiments

Chronoamperometric transients were achieved using a sample time of 0.1 s. The potential was held at 0 V for 20 s for pre-treatment, then the potential was stepped to the required value and the current was measured for 10 s. Fitting of the experimental data was achieved using the non-linear curve fitting function available in Origin 7.0 (MicroCal Software Inc.), following the Shoup and Szabo[24] approximation, as employed by Evans *et al.*[25] The equations used in this approximation are sufficient to describe the current response to within an accuracy of 0.6%, and are given below:

$$I = -4nFDcr_{d}f(\tau) \quad (2)$$

$$f(\tau) = 0.7854 + 0.8863\tau^{-\frac{1}{2}} + 0.2146e^{-0.7823\tau^{-\frac{1}{2}}} \quad (3)$$

$$\tau = \frac{4Dt}{r_{d}^{2}} \quad (4)$$

where n is the number of electrons transferred, F is the Faraday constant, D is the diffusion coefficient, c is the bulk concentration of the parent species, r_d is the radius of the microdisk, and t is the time.

The software was instructed to perform 100 iterations on the data, fixing the value for the electrode radius, which was previously calibrated. When the experimental data had been optimised, a value for the diffusion coefficient, D, and the product of the number of electrons multiplied by the concentration, nc, was obtained.

Results and discussion

The RTIL chosen as the solvent for this study was $[C_2mim][NTf_2]$ (see Fig. 1 for structure), since this showed a wide electrochemical window in excess of 5.5 V, and no obvious electrochemical features when fully degassed. $[C_4mim][NO_3]$ was then chosen as a source of nitrate ions, as it is liquid at room temperature and less hygroscopic than solid $[C_2mim][NO_3]$. It is thought that the different nature of the cation will have little/no effect on the voltammetry presented below.

Fig. 2 shows the oxidation of nitrate ions (from $[C_4mim][NO_3]$) in the RTIL $[C_2mim][NTf_2]$ on a Pt microelectrode (diameter 10 μm) at concentrations of 141, 275, 524 and 1153 mM. A plot of peak current *vs.* concentration (inset of Fig. 2)

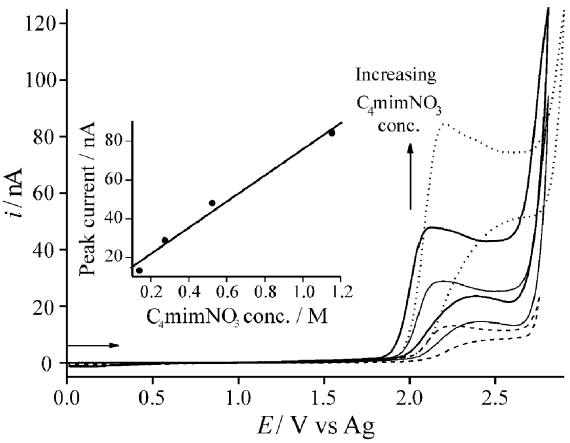

Fig. 2 Cyclic voltammograms for the oxidation of $[C_4mim][NO_3]$ (concentrations of 141, 275, 524 and 1153 mM) in the RTIL $[C_2mim][NTf_2]$ on a Pt microelectrode (diameter 10 μm). Scan rate: 1 V s^{-1}. The inset shows a plot of nitrate concentration *vs.* peak current (line of best fit: $r^2 = 0.98$).

was found to be approximately linear, and the relatively large peak currents reflect the high solubility of $[C_4mim][NO_3]$ in $[C_2mim][NTf_2]$. The oxidation occurs at a high positive potential, in excess of +2 V, which is not surprising given the already high oxidation state of the ion. To the best of our knowledge, there are no reports of any similar voltammetric peaks in the literature, since, in conventional solvents, the peak is obscured by earlier solvent breakdown on platinum electrodes. The wide electrochemical window of this particular ionic liquid allows the observation of this peak, which is not even seen in melts of nitrate salts.[8,10] The shape of this peak appears sharp at 100 mV s^{-1}, even on a small microelectrode, but becomes close to steady-state at scan rates of 10 mV s^{-1} and below (not shown here). This is a reflection of the higher viscosity (and hence slower diffusion) of the RTIL compared to conventional solvents, where steady-state behaviour would be expected at 100 mV s^{-1} on such a small microelectrode.

A potential step was carried out on the oxidative peak for all the concentrations studied. The potential was stepped from 0 V (corresponding to no faradaic current) to a potential after the nitrate oxidation peak. The chronoamperometric transients were theoretically fit to the Shoup and Szabo[24] expression and in all cases, gave a very good fit (±0.7%) to the experimental results. The analysis of the transients gives a range of diffusion coefficients (1.17 to 1.90 × 10^{-11} m^2 s^{-1}) for the nitrate ion, which arises due to the different viscosities of the two liquids that make up the mixture (28 cP for $[C_2mim][NTf_2]$, and 228 cP for $[C_4mim][NO_3]$, at 293 K). Fig. 3 shows a plot of the diffusion coefficients (obtained from the best theoretical fit to the experimental data) *vs.* concentration of $[C_4mim][NO_3]$, and will be discussed later. The results from transient analysis also gave a combined value for the number of electrons, n, multiplied by concentration, c. Since c is known, these results indicate a one-electron process, suggesting that the oxidation follows a previously proposed[8] mechanism:

$$NO_3^- \rightarrow NO_2 + \tfrac{1}{2}O_2 + e^- \quad (5)$$

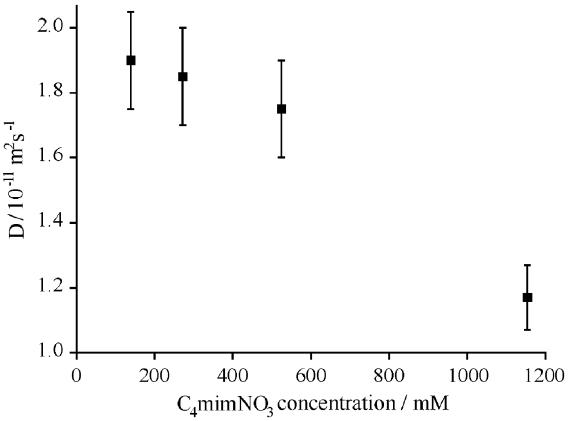

Fig. 3 Plot of diffusion coefficients, D, against concentration, c, of $[C_4mim][NO_3]$ in $[C_2mim][NTf_2]$. Average D and c values were obtained from fitting to chronoamperometric transients, and error bars were calculated from 3-D contour plots of mean-squared absolute deviation.[27] D = 1.9 (±0.15), 1.85 (±0.15), 1.75 (±0.15) and 1.17 (±0.10) × 10^{-11} m^2 s^{-1}, respectively.

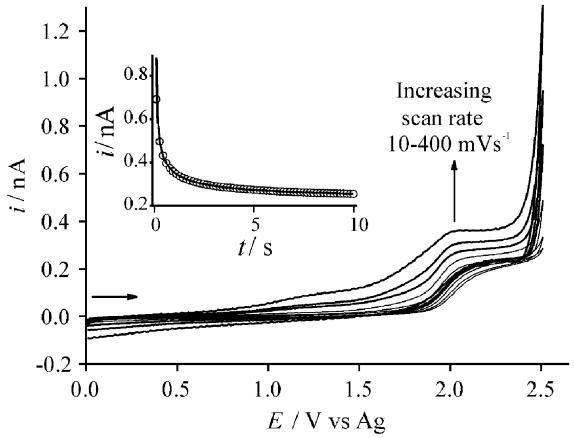

Fig. 4 Cyclic voltammograms for the oxidation of a saturated solution of $NaNO_3$ in the RTIL $[C_2mim][NTf_2]$ on a Pt microelectrode (diameter 10 μm) at scan rates of 10, 20, 50, 100, 200 and 400 mV s^{-1}. The inset shows the experimental (—) and fitted theoretical (○) chronoamperometric transients for the oxidation of $NaNO_3$ in $[C_2mim][NTf_2]$. The potential was stepped from 0 to +2.3 V.

The highly chemically irreversible shape of the oxidation peak indicates that the electrochemical step must be accompanied by a chemical reaction, further supporting eqn (5). The gaseous products (nitrogen dioxide and oxygen) must then diffuse very quickly from the electrode surface, which explains why no reductive "back" peaks were observed on the reverse sweep in the potential range +2.0 to −2.0 V (*cf.* reduction potential of oxygen in $[C_2mim][NTf_2]$ is −1.2 V *vs.* Ag)[26] at all scan rates studied (5–4000 mV s^{-1}).

Three-dimensional surface (contour) plots were constructed for the four concentrations, following the mean-scaled absolute deviation, as employed in ref. 27. The contour plots revealed single minima in all cases, indicating that there is only one set of optimised values for the diffusion coefficient, D, and the concentration, c. As a result of this analysis, error bars have been added to the plot in Fig. 3, indicating a small range in D, and a negligible range in c. For the more concentrated solution, the diffusion coefficient was the lowest, as expected from the larger volume of more viscous $[C_4mim][NO_3]$ present in the mixed solution. We can estimate from the graph that the diffusion coefficient of $[C_4mim][NO_3]$ in $[C_4mim][NTf_2]$ at infinite dilution is *ca.* 2 × 10^{-11} m^2 s^{-1}.

We next looked at the oxidation of both sodium nitrate ($NaNO_3$) and potassium nitrate (KNO_3) separately in $[C_2mim][NTf_2]$. Fig. 4 shows typical cyclic voltammograms obtained over a range of scan rates (10–400 mV s^{-1}) for the oxidation of a saturated solution of $NaNO_3$ in $[C_2mim][NTf_2]$ on a 10 μm diameter Pt electrode. The peak currents observed are much smaller than for $[C_4mim][NO_3]$ in $[C_2mim][NTf_2]$, despite the RTIL solution being saturated with $NaNO_3$. The shapes of the peaks are also more steady-state like, suggesting the possibility of ion pairing (see below), or a result of the lower concentration of $NaNO_3$ compared to $[C_4mim][NO_3]$. The latter effect was observed in Fig. 2 for the oxidation of $[C_4mim][NO_3]$ in $[C_2mim][NTf_2]$; the oxidation peaks became more transient shaped at higher concentrations.

In order to calculate the concentration (solubility) of sodium nitrate, a potential step experiment was performed. The potential was stepped from 0 V (no faradaic current) to a potential after the peak, and the current was monitored for 10 s. The resulting chronoamperometric transient is shown in the inset of Fig. 4, with the experimental data (—) giving excellent agreement (±0.7%) with the theoretically derived data (○) from the Shoup and Szabo[24] expression. The diffusion coefficient of $NaNO_3$ in $[C_2mim][NTf_2]$ at 298 K was calculated to be 8.8 (±0.8) × 10^{-12} m^2 s^{-1} (after analysis of the three-dimensional contour plot), which is approximately 1–2 orders of magnitude smaller than that obtained in aqueous[28] solutions (1.5 × 10^{-9} m^2 s^{-1} at 298 K), and is reasonable considering the higher viscosity of the RTIL compared to water. The results also suggest a concentration (or solubility) of $NaNO_3$ of 11.9 (±0.5) mM in $[C_2mim][NTf_2]$, and this modest value is consistent with the relatively small peak currents obtained in Fig. 4.

Analogous experiments were carried out for the oxidation of KNO_3. Fig. 5 shows cyclic voltammograms for the oxidation of a saturated solution of KNO_3 in $[C_2mim][NTf_2]$ on a Pt electrode (diameter 10 μm) at scan rates of 10–400 mV s^{-1}. The shape and position of the wave is almost identical to that obtained for $NaNO_3$ (Fig. 4). The results from chronoamperometric fitting (Fig. 5 inset) and contour analysis give a diffusion coefficient for KNO_3 of 9.0 (±0.6) × 10^{-12} m^2 s^{-1} (compared to 1.2–1.9 × 10^{-9} m^2 s^{-1} in water[29] at 298 K), and a modest concentration, or solubility, of 10.8 (±0.3) mM. The low solubility of both $NaNO_3$ and KNO_3 in $[C_2mim][NTf_2]$ may prove to be a disadvantage if this technique is to be applied to the analytical determination of these compounds in RTILs. When comparing the diffusion coefficients of $NaNO_3$ and KNO_3 to that obtained for $[C_4mim][NO_3]$ (see above), it is obvious that, even with experimental error, the diffusion coefficients for the nitrate ion in the sodium and potassium compounds are much lower than in $[C_4mim][NO_3]$. This observation indicates that the nitrate ion may be ion-paired to Na^+ or K^+, leading to slower diffusion of

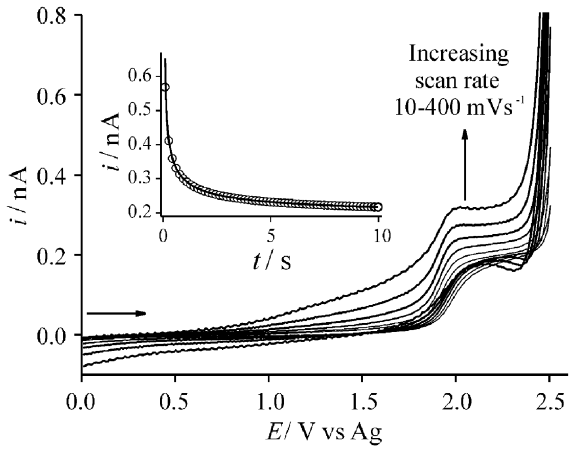

Fig. 5 Cyclic voltammograms for the oxidation of a saturated solution of KNO_3 in $[C_2mim][NTf_2]$ on a Pt microelectrode (diameter 10 μm) at scan rates of 10, 20, 50, 100, 200 and 400 mV s^{-1}. The inset shows the experimental (—) and fitted theoretical (○) chronoamperometric transients for the oxidation of KNO_3 in $[C_2mim][NTf_2]$. The potential was stepped from 0 to +2.2 V.

$NaNO_3$ and KNO_3, and supports the suggestion of formation of Na_2O and K_2O as products of the reduction (see later).

Next, the reduction of both species was studied. Fig. 6 shows a typical cyclic voltammogram for the reduction of a saturated solution of $NaNO_3$ in $[C_2mim][NTf_2]$ on a Pt electrode (diameter 10 μm) at a scan rate of 1 V s^{-1}. The reduction is suggested to follow the mechanism:

$$2Na^+ + NO_3^- + 2e^- \rightarrow Na_2O + NO_2^- \qquad (6)$$

The reduction is not peak-shaped (in contrast with $NaNO_3$ melts),[7–9,11] but the onset of the reduction occurs well before the edge of the RTIL solvent window. A current of approximately −240 nA was chosen as a limiting value for reversal of the voltammetric sweep. On the reverse sweep, several anodic features are observed. The inset to Fig. 6 shows a close-up view of the voltammetry in a reduced current range. Five distinctive peaks are observed, and the identities of peaks i to v

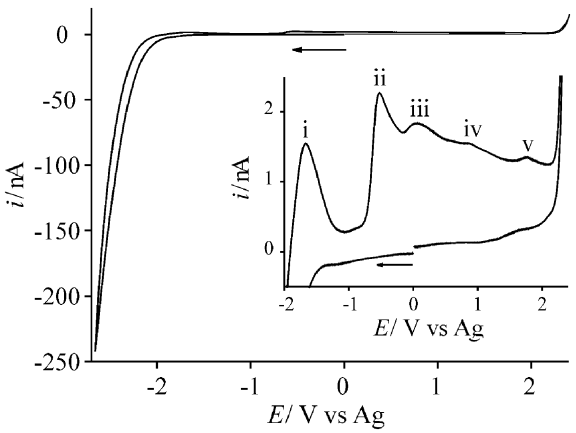

Fig. 6 Cyclic voltammetry for the reduction of a saturated solution of $NaNO_3$ in $[C_2mim][NTf_2]$ at a Pt microelectrode (diameter 10 μm). Scan rate: 1 V s^{-1}.

Table 1 Summary of the proposed reactions and peak assignments (Fig. 6, Fig. 7 and Fig. 8) following the reduction of $NaNO_3$ and KNO_3

Peak			
$NaNO_3$	KNO_3	Proposed reaction[a]	Equation
i	I	$2M_2O \leftrightharpoons M_2O_2 + 2M^+ + 2e^-$	(7)
ii	II	$M_2O_2 \leftrightharpoons MO_2 + M^+ + e^-$	(8)
iii	III	$MO_2 \leftrightharpoons O_2 + M^+ + e^-$	(9)
iv	IV	$NO_2^- \rightarrow NO_2 + e^-$	(10)
v	V	$NO_3^- \rightarrow NO_2 + \frac{1}{2}O_2 + e^-$	(5)
iii″		$O_2 + e^- + M^+ \leftrightharpoons MO_2$	(11)
ii″		$MO_2 + e^- + M^+ \leftrightharpoons M_2O_2$	(12)

[a] $M = Na^+$ or K^+.

are suggested in Table 1, based on similar observations in $NaNO_3$ melts.[7–9] We propose that the peak observed at −1.67 V *vs.* Ag in Fig. 6 corresponds to the oxidation of sodium oxide (Na_2O) to sodium peroxide (Na_2O_2), which is followed at −0.52 V by the oxidation of sodium peroxide to sodium superoxide (NaO_2), and further by the oxidation of sodium superoxide to molecular oxygen at +0.06 V. We also suggest that peak iv at +0.87 V *vs.* Ag is the oxidation of sodium nitrite ($NaNO_2$), since a separate study of $NaNO_2$ in $[C_2mim][NTf_2]$ (not shown here) showed an oxidation peak in almost the same position *vs.* a silver quasi-reference electrode (QRE). The identification also seems reasonable, since $NaNO_2$ is formed in the reduction shown by eqn (1). Peak v at +1.77 V likely corresponds to the oxidation of $NaNO_3$, initially present in the solution, which has shifted to a slightly more negative value than in Fig. 3, possibly due to either a slight drift in the Ag QRE, or a catalysing effect due to, for example, a Na_2O film/precipitate on the electrode surface, which has been previously reported.[9–11] All equations describing peaks i to v are given in Table 1.

The same experiments were repeated for potassium nitrate. Fig. 7 shows a typical cyclic voltammogram for the reduction of a saturated solution of KNO_3 in $[C_2mim][NTf_2]$ on a 10 μm Pt electrode at a scan rate of 1 V s^{-1}. The onset of the reduction begins at a slightly more negative potential than for $NaNO_3$, but the shape is generally the same. The scan was reversed when the current reached −240 nA, and several features were observed on the anodic sweep. A close-up view of these features is shown in the inset of Fig. 7. As with $NaNO_3$, we propose that peak I at −1.18 V is the oxidation of the oxide (K_2O), peak II at −0.38 V is the oxidation of K_2O_2, peak III at +0.18 V is the oxidation of KO_2, peak IV at +0.82 V is the oxidation of nitrite and peak V at +1.92 V is the oxidation of nitrate. All equations for the peak assignments are given in Table 1.

It seems logical to compare the relative sizes of the anodic peaks obtained for the reductions of $NaNO_3$ and KNO_3 (Fig. 6 and Fig. 7) in terms of the known stability of the species. For both $NaNO_3$ and KNO_3 in $[C_2mim][NTf_2]$, all three species (oxide, peroxide and superoxide) are observed. The most thermodynamically stable sodium product is known to be the peroxide, Na_2O_2,[7,8,30] which is reflected well by the peak heights in Fig. 6 (the oxidation peak (ii) of Na_2O_2 is the largest). However, the most thermodynamically stable

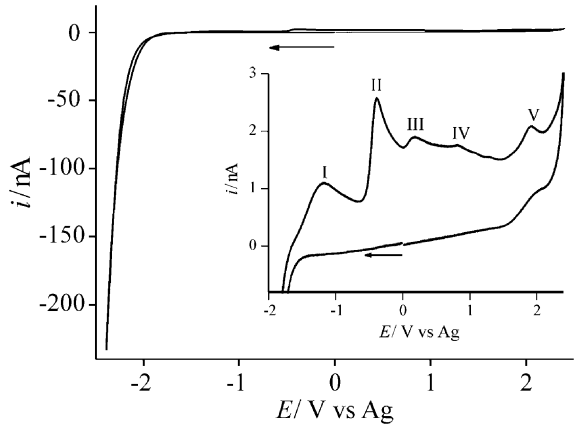

Fig. 7 Cyclic voltammetry for the reduction of a saturated solution of KNO_3 in $[C_2mim][NTf_2]$ at a Pt microelectrode (diameter 10 μm). Scan rate: 1 V s^{-1}.

potassium species is predicted to be the superoxide KO_2,[7,8,30] which is *not* represented well by the peak heights in Fig. 7. Instead, the peak representing K_2O_2 oxidation (II) has the largest
peak current, indicating that potassium peroxide is the most stable in this RTIL medium. Furthermore, the most notable difference of the two figures is that the sodium oxide peak (i) is relatively large compared to the potassium oxide peak (I), suggesting that Na_2O is more readily formed than K_2O.

Fig. 8 shows repeat voltammetric cycles for the reduction of a saturated solution of $NaNO_3$ under the same conditions as in Fig. 6. Five consecutive scans are shown, with the first scan shown for clarity as dots. As can be clearly seen, on consecutive scans, the onset of the reduction shifts to a slightly more negative potential and the heights of all three anodic peaks decrease. The decrease in peak heights is most likely due to the lower current maxima reached on successive scans. We

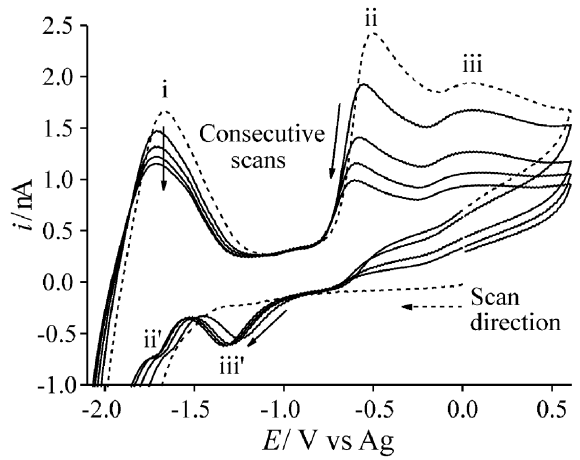

Fig. 8 Cyclic voltammetry for the reduction of a saturated solution of $NaNO_3$ in $[C_2mim][NTf_2]$ at a Pt microelectrode (diameter 10 μm) with a reduced anodic limit of +0.5 V. The first scan (···) and 4 subsequent scans (—) are shown at a scan rate of 1 V s^{-1}.

also observe that the height of the peroxide and superoxide peaks (ii) and (iii) decrease by a greater extent than the oxide peak (i), indicating some build-up of disodium(I) oxide on the electrode surface. The formation of a Na_2O precipitate in a pure $NaNO_3$ melt is well documented in the literature.[9–11] The second observation is the appearance of two new cathodic peaks, ii′ and iii′, labelled with the same numbers as the anodic peaks to which they relate. When the cycles are reversed at −0.25 V, peak iii′ is not observed, but the small peak ii′ is still present (although smaller). We therefore identify peak iii′ as the reduction of oxygen to superoxide (eqn (11)), and peak ii′ as the reduction of superoxide to peroxide (eqn (12)). This effect has also been noted previously.[7,9] We then observed some evidence of fouling/deposition on the electrode after the appearance of the two extra peaks; peaks iii′ and ii′ were present on the first scan, even after the electrode was left for 30 min to equilibrate under high vacuum conditions. Polishing of the electrode was required to restore the platinum surface to its original state.

Due to the useful hydrogen storage properties of disodium(I) oxide,[12] it would be advantageous to confirm if the reduction of $NaNO_3$ results in the electrodeposition of Na_2O on the electrode surface. Therefore, further studies were performed on the saturated solution of $NaNO_3$. The heights of the peaks from the voltammetry (Fig. 6) suggest that all three species, Na_2O, Na_2O_2 and NaO_2, are present after the reduction, but do not shed light on the identity, if at all, of any deposit. In order to confirm the presence or absence on the electrode surface of any of these species (disodium(I) oxide, sodium peroxide or sodium superoxide) using XPS, a larger platinum disk electrode was constructed (see experimental). The reduction of the saturated solution of $NaNO_3$ (as in Fig. 6) was first repeated with this larger electrode, to ensure that the same reactions were taking place. The voltammetry showed similar features to that obtained with the 10 μm diameter Pt microelectrode, and so was not included here. The potential was then swept from 0 V to −2.8 V, and held for 10 min in order to maximise any deposition that might be taking place. We briefly note here that after 10 min deposition time, the $NaNO_3$–RTIL solution changed from colourless to a deep yellow-brown colour, and increased the height of all anodic peaks by *ca.* 50%.

Fig. 9 shows an XPS spectrum of the electrodeposited electrode. The figure is labelled with the peaks corresponding to the atoms that make up the structure of the RTIL (see Fig. 1). Initially, the XPS spectrum obtained from the electrode was swamped by C, N, O, F and S peaks from the ionic liquid. Once the electrode was vigorously sprayed with acetone, the resultant spectrum showed a clear platinum peak at a binding energy of 71.1 eV (charge compensated and corrected), and a sodium (Na 1s) signal at 1072.6 eV (also labelled on Fig. 9). In order to identify the sodium deposit, two standards, sodium oxide and sodium peroxide were also studied. The binding energy of the standards were as follows: sodium oxide 1073.6 eV, and sodium peroxide 1071.6 eV. The small deviation in binding energy from the standards may be due to the deposited species partially oxidising in air during the transfer process. These results indicate that the species present on the platinum surface is sodium oxide, Na_2O.

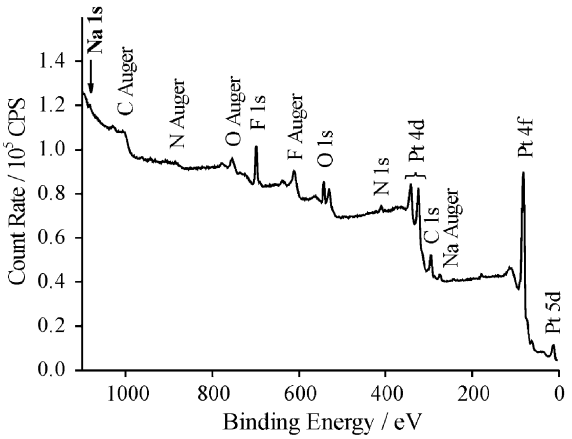

Fig. 9 Survey scan XPS spectrum of the surface of a 6 mm diameter Pt electrode (after 10 min electrochemical deposition time in a saturated solution of $NaNO_3$ in [C_2mim][NTf_2]). The peaks from the constituent atoms that make up the RTIL (C, N, O, F), and the Na (1s) and Pt (4f, 4d and 5d) peaks are all labelled.

Conclusions

By dissolving the solids of sodium nitrate and potassium nitrate in a common RTIL [C_2mim][NTf_2], several observations were made. (1) The wide electrochemical window of [C_2mim][NTf_2] has allowed the observation of a clear oxidation peak, and easy calculation of concentrations and diffusion coefficients of both $NaNO_3$ and KNO_3. This work may have applications in the electrochemical determination of nitrate ions, although the low solubility in RTILs could prove to be a limiting factor. (2) The voltammetric features observed for the reduction of $NaNO_3$ and KNO_3 were almost identical to that obtained in melts at temperatures of 350–500 °C. Without the need for such extreme conditions, studies of other melts may be significantly more facile by simply dissolving them in an RTIL. (3) XPS studies have also revealed that sodium oxide is likely electrodeposited on the platinum electrode in a $NaNO_3$–RTIL solution.

Acknowledgements

DSS thanks Schlumberger Cambridge Research and LA thanks the Department of Education and Learning in Northern Ireland and Merck GmBH for financial support.

References

1 (*a*) M. J. Moorcroft, J. Davis and R. G. Compton, *Talanta*, 2001, **54**, 785–803; (*b*) J. Davis, M. J. Moorcroft, S. J. Wilkins, R. G. Compton and M. F. Cardosi, *Analyst*, 2000, **125**, 737–742; (*c*) D. Pletcher and Z. Poorabed, *Electrochim. Acta*, 1979, **24**, 1253–1256.
2 G. E. Dima, A. C. A. de Vooys and M. T. M. Koper, *J. Electroanal. Chem.*, 2003, **554–555**, 15–23.
3 M. S. El-Deab, *Electrochim. Acta*, 2004, **49**, 1639–1645.
4 I. Taniguchi, N. Nakashima, K. Matsushita and K. Yasukouchi, *J. Electroanal. Chem. Interfacial Electrochem.*, 1987, **224**, 199–209.
5 (*a*) M. T. de Groot and M. T. M. Koper, *J. Electroanal. Chem.*, 2004, **562**, 81–94; (*b*) M. Fedurco, P. Kedzierzawski and J. Augustynski, *J. Electrochem. Soc.*, 1999, **146**, 2569–2572; (*c*) S. J. Hsieh and A. A. Gewirth, *Langmuir*, 2000, **16**, 9501–9512.
6 A. N. Fletcher, M. H. Miles and M. L. Chan, *J. Electrochem. Soc.*, 1979, **126**, 1496–1501.
7 K. E. Johnson and P. S. Zacharias, *J. Electrochem. Soc.*, 1977, **124**, 448–450.
8 M. Miles and A. N. Fletcher, *J. Electrochem. Soc.*, 1980, **127**, 1761–1766.
9 P. G. Zambonin, *J. Electroanal. Chem. Interfacial Electrochem.*, 1970, **24**, 365–377.
10 H. E. Bartlett and K. E. Johnson, *J. Electrochem. Soc.*, 1967, **114**, 64–67.
11 H. S. Swofford, Jr and H. A. Laitinen, *J. Electrochem. Soc.*, 1963, **110**, 814–820.
12 Q. Xu, R. Wang, T. Kiyobayashi, N. Kuriyama and T. Kobayashi, *J. Power Sources*, 2006, **155**, 167–171.
13 (*a*) M. C. Buzzeo, R. G. Evans and R. G. Compton, *ChemPhysChem*, 2004, **5**, 1106–1120; (*b*) D. S. Silvester and R. G. Compton, *Z. Phys. Chem.*, 2006, **220**, 1247–1274; (*c*) F. Endres and S. Zeil El Abedin, *Phys. Chem. Chem. Phys.*, 2006, **8**, 1–16.
14 P. C. Howlett, D. R. MacFarlane and A. F. Hollenkamp, *Electrochem. Solid-State Lett.*, 2004, **7**, A97–A101.
15 M. C. Buzzeo, C. Hardacre and R. G. Compton, *Anal. Chem.*, 2004, **76**, 4583–4588.
16 A. B. McEwen, H. L. Ngo, K. LeCompte and J. L. Goldman, *J. Electrochem. Soc.*, 1999, **146**, 1687–1698.
17 P. Wang, S. M. Zakeeruddin, J. E. Moser and M. Grätzel, *J. Phys. Chem. B*, 2003, **107**, 13280–13285.
18 P. Bonhôte, A.-P. Dias, N. Papageorgiou, K. Kalyanasundaram and M. Grätzel, *Inorg. Chem.*, 1996, **35**, 1168–1178.
19 L. Cammarata, S. G. Kazarian, P. A. Salter and T. Welton, *Phys. Chem. Chem. Phys.*, 2001, **3**, 5192–5200.
20 U. Schröder, J. D. Wadhawan, R. G. Compton, F. Marken, P. A. Z. Suarez, C. S. Consorti, R. F. de Souza and J. Dupont, *New J. Chem.*, 2000, **24**, 1009–1015.
21 M. Sharp, *Electrochim. Acta*, 1983, **28**, 301–308.
22 D. A. Shirley, *Phys. Rev. B: Solid State*, 1972, **5**, 4709–4714.
23 D. Briggs and M. P. Seah, in *Practical Surface Analysis, Vol 1: Auger and X-ray Photoelectron Spectroscopy*, D. Briggs and M. P. Seah, Wiley, Chichester, 2nd edn, 1990, pp. 531–540.
24 D. Shoup and A. Szabo, *J. Electroanal. Chem. Interfacial Electrochem.*, 1982, **140**, 237–245.
25 R. G. Evans, O. V. Klymenko, S. A. Saddoughi, C. Hardacre and R. G. Compton, *J. Phys. Chem. B*, 2004, **108**, 7878–7886.
26 M. C. Buzzeo, O. V. Klymenko, J. D. Wadhawan, C. Hardacre, K. R. Seddon and R. G. Compton, *J. Phys. Chem. A*, 2003, **107**, 8872–8878.
27 N. Fietkau, A. D. Clegg, R. G. Evans, C. Villagrán, C. Hardacre and R. G. Compton, *ChemPhysChem*, 2006, **7**, 1041–1045.
28 (*a*) H. S. Harned and J. A. Shropshire, *J. Am. Chem. Soc.*, 1958, **80**, 2618–2619; (*b*) H. S. Yeh and G. B. Willis, *J. Chem. Eng. Data*, 1970, **15**, 187–189.
29 V. Daniel and J. G. Albright, *J. Solution Chem.*, 1991, **20**, 633–642.
30 D. F. Shriver, P. W. Atkins and C. H. Langford, *Inorganic Chemistry*, Oxford University Press, Oxford, UK, 1990.

